Progress In Electromagnetics Research, PIER 35, 315–334, 2002

NUMERICAL STUDIES OF LEFT HANDED METAMATERIALS

C. D. Moss, T. M. Grzegorczyk, Y. Zhang, and J. A. Kong

Research Laboratory of Electronics
Massachusetts Institute of Technology
Cambridge, MA 02139-4307, USA

Abstract—We use the three dimensional Finite Difference Time Domain (FDTD) technique to study metamaterials exhibiting both negative permittivity and permeability in certain frequency bands. The structure under study is the well-known periodic arrangement of rods and split-ring resonators, previously used in experimental setups. The three parameters we study are the transmission coefficient of a slab, the phase variation of the propagating fields within the metamaterial, and the refraction of a wave through a prism. To our knowledge, this is the first time that the last two parameters are studied rigorously using a numerical method. The results of this work show that fields propagating inside the metamaterial with a forward power direction exhibit a backward phase velocity and negative index of refraction.

1. INTRODUCTION

Materials exhibiting negative permittivity and permeability are a popular topic of current research due to their recent physical realization as metamaterials [1]. Recent research has focused both on the behavior of these metamaterials as well as on the incorporation of negative permittivity and permeability into electromagnetic theory [2].

The key theoretical aspects and some applications were first investigated by Veselago in 1968 [3]. In his pioneering work, Veselago introduced the nomenclature 'left-handed (LH) materials', to refer to the left-handed dyad formed by the electric field ($\overline{E}$), magnetic field ($\overline{H}$), and wave vector ($\overline{k}$). Veselago predicted LH properties such as a reversed Doppler effect, reversed Čerenkov radiation, and a negative index of refraction. To date, the range of imaginable applications extends to the field of antenna design, vehicle coatings for altering radar cross section properties, and lenses [4].

Currently, the metamaterials under study are composed of a periodic arrangement of metallic printed lines (or rods) that exhibit a negative permittivity, and split-ring resonators (SRRs) that exhibit a negative permeability. To understand how these metamaterials function, it is best to follow the historical steps that lead to the current geometry. First, it was shown that a 3D array of thin, continuous (very long) metal wires exhibit a resonant frequency response similar to that of a plasma medium [5, 6]. At frequencies below the resonant frequency, the permittivity becomes negative, the wave vector is imaginary, and there is no transmission. Above the resonant frequency, the permittivity is real and transmission occurs. Second, it was demonstrated that negative permeability could be achieved using an array of SRRs [7]. The SRRs act like magnetic dipoles, with a resonant response resulting from internal inductance and capacitance. Close to resonance, the SRRs produce strong magnetic fields whose directions oppose the incident magnetic field, resulting in a negative effective permeability. Finally, once the negative permeability structures had been discovered, finding ways of combining them with negative permittivity structures was the next step in research, leading to the well known geometry shown in [1].

However, the demonstration of the LH properties of a metamaterial is not as straightforward as it seems, and showing that permittivity and permeability are separately negative over a similar frequency band does not imply that they remain so when the rods and SRRs are combined into a unique geometry. One of the first observations of the LH nature of these metamaterial structures was inferred by observing transmission and reflection coefficients over

a wide frequency band. For the separate geometries (rods only or SRRs only), no transmission occurs because of an imaginary wave number. In the frequency band where the two parameters are simultaneously negative, transmission occurs when the combined geometry is considered. This band-pass phenomenon was indeed observed in these metamaterials [1]. However, as mentioned before, this transmission is not sufficient to conclude that the material is exhibiting LH behavior, since the interaction between the SRRs and rods could result in a positive permittivity and permeability, which would also yield transmission. A more rigorous test to demonstrate the LH nature of a material is therefore to either directly measure the phase inside the material (this can be done numerically, as will be shown later, but is very difficult to realize practically), or to measure the index of refraction of a prism. Snell's law dictates that the angle of transmission into or out of any right-handed (RH, with positive permittivity and permeability) material must be on the opposite side of the surface normal with respect to the incident angle. For LH materials, however, the angle of transmission is on the same side of the normal, which has been theoretically demonstrated and experimentally verified [3, 8]. Note that recent work has suggested another rigorous way of calculating the index of refraction of a LH slab by measuring the lateral shift of an incident Gaussian beam [9].

Previous numerical modeling has been carried out to study the fields inside homogeneous LH materials in waveguides [10], as well as stratified LH media [2]. Numerical modeling of the metamaterials has been restricted to transmission and reflection coefficient measurements [11], or fields around a single SRR or periodic array of SRRs [13]. To date, little work has been done to investigate and verify the LH behavior of fields propagating within these metamaterials. Furthermore, only experimental work has been carried out to show the refraction from a prism with a negative index of refraction.

The purpose of this work is to use the three dimensional FDTD method to study the transmission characteristics, phase propagation, and index of refraction of metamaterials to unambiguously determine their LH or RH property. Two macroscopic configurations of metamaterials are used towards this purpose: a slab to calculate the transmission coefficient and phase propagation, and a prism to study the index of refraction. The microscopic configurations of all the metamaterials are similar, based on the periodic arrangement of rods and SRRs [1], embedded in a parallel plate waveguide.

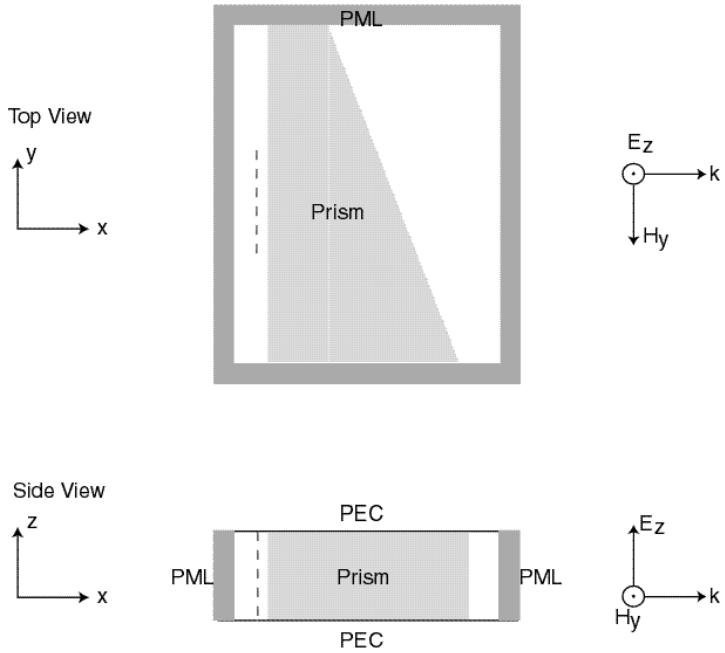

Figure 1. FDTD computational domain: a metamaterial structure (prism in this case) is included in a PEC parallel plate waveguide with PML lateral boundaries. Source is a current sheet approximating a horn antenna.

2. FDTD MODEL

We have based our numerical model on the experimental setup published in [8]. The FDTD computational domain is shown in Figure 1, modeling a metamaterial in a parallel plate waveguide. The structure can be either a slab or a prism (Figure 1), depending on the type of study performed. The parallel plates are perfect electrically conducting (PEC) sheets. Surrounding the structure is a Perfectly Matched Layer (PML) [13] that models microwave absorber, and ensures that reflections are small. In the model, the source is a current sheet that approximates a TE_{10} horn antenna, shown in Figure 1 as a dashed line. The current sheet radiates both forward and backward, but the wave traveling away from the structure is absorbed by the PML.

The model chosen for the SRRs is shown in Figure 2(a), with a discretization size of 0.25 mm. For an FDTD grid with a uniform cell size, the model of the exact geometry used in the experiment [8]

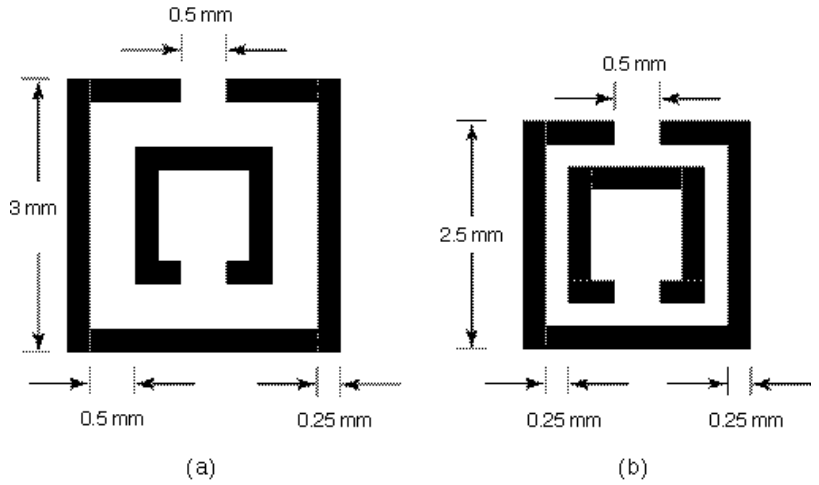

Figure 2. FDTD model of the split ring resonators, using discretizations of (a) 0.25 mm, (b) 0.125 mm.

requires finer discretization and thus many more unknowns. The new geometry of Figure 2(a) will likely exhibit a different resonant frequency. The SRRs and rods are modeled as PEC materials in the standard fashion by setting the tangential electric fields to zero. For the sake of comparison with the experimental setup, results are also presented for the SRR model shown in Figure 2(b), which is closer to [8] and attained through a finer discretization of 0.125 mm.

The metamaterial consists of a periodic array of unit cells. A unit cell of the structure, in one plane, is shown in Figure 3(a). As in the experimental setup, we have chosen three SRRs stacked vertically between the PEC waveguide plates, printed on one side of a dielectric substrate (ϵ_r). On the other side of the substrate is printed a metallic rod 0.5 mm wide. A unit cell measures 5 mm $\times$ 5 mm $\times$ 13 mm. Using many unit cells in a single plane alone would create an anisotropic metamaterial, coupling with only one magnetic field component. Following [8], in order to create a more isotropic metamaterial, a structure in two planes is created as shown in Figure 3(b), where the unit cell is repeated in the ($\hat{x}$,$\hat{z}$) and ($\hat{y}$,$\hat{z}$) planes. In this case, the SRRs interact with both the $\hat{x}$ and $\hat{y}$ magnetic fields, while the rods still couple with the $\hat{z}$ electric field. The structure shown in Figure 3(b) is a 2 $\times$ 2 array of SRRs, and is a typical example of the types of structures that are examined in the following sections.

For most of the following results, we study a metamaterial

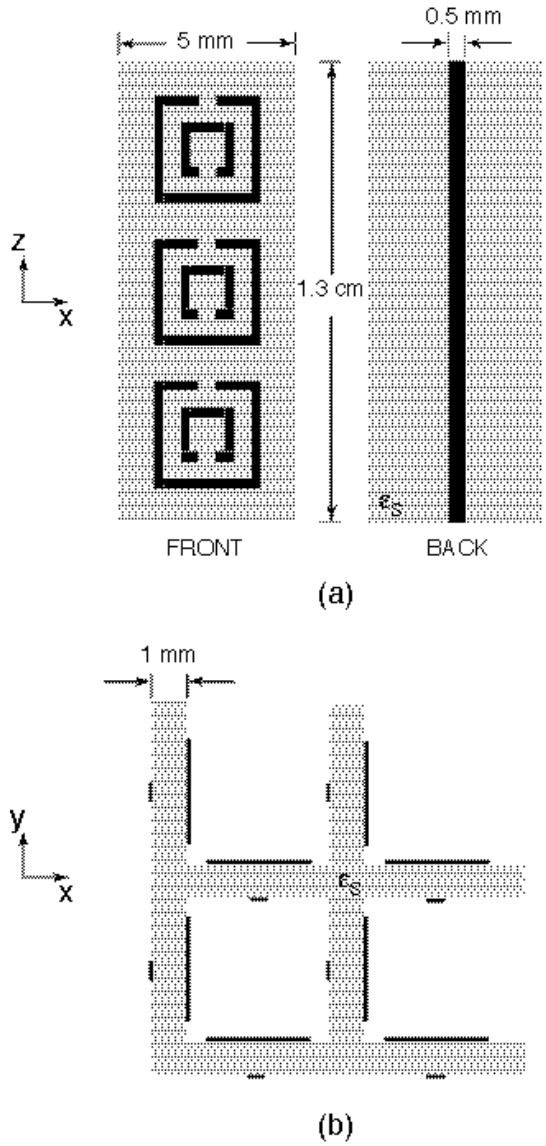

Figure 3. (a). Front and back of a single set of split ring resonators and rod. (b) 2 × 2 array of SRRs and rods.

structure containing 9 × 12 unit cells. The computational domain measures 4.75 cm × 6.25 cm × 1.3 cm, or 190 × 250 × 52 cells, not including the PML. For the discretization of 0.25 mm, the corresponding time step is 4.77×10^{-4} ns. One simulation requires approximately 14 million unknowns to be solved, and it takes about 1.5 hours to complete 4000 time steps on a 667 MHz DEC Alpha Server with 4 GB of RAM.

3. RESULTS

The FDTD model described in the previous section is used to perform three types of simulations. First, it is necessary to determine frequencies at which negative permittivity and permeability might exist. This is done by calculating the transmission coefficient of the metamaterial, and looking for band-pass regions. Once these frequencies are found, a continuous wave is used to examine the phase advance through the structure. Finally, at the same frequencies, a prism is used to calculate the index of refraction of the structure.

Four types of metamaterial are studied:

- Type 1: the structure shown in Figure 3(b) with the substrate $\epsilon_r = 1.0$; SRR geometry shown in Figure 2(a).
- Type 2: Figure 3(b) with $\epsilon_r = 3.4$; SRR geometry shown in Figure 2(a).
- Type 3: Figure 3(b) with SRRs and rods in the $(\hat{x},\hat{z})$ plane only, $\epsilon_r = 1.0$; SRR geometry shown in Figure 2(a).
- Type 4: Figure 3(b), with $\epsilon_r = 1.0$; SRR geometry shown in Figure 2(b).

3.1. Determining Frequencies of LH Behavior

Determining the transmission coefficient of the metamaterial can be done in the FDTD model by using a wideband pulse incident on a metamaterial slab. For our simulations, we use the first derivative of a Blackmann-Harris pulse [14] that vanishes completely after time period $T = 1.55/f_c$ ($f_c = 12$ GHz).

Figure 4 shows the transmission coefficient of the Type 1 structure. Three cases are shown, for a periodic arrangement of rods alone (without SRRs), for the SRRs alone (without rods), and for the entire structure containing both the rods and SRRs. The structure with the rods alone has a high pass filter behavior, with transmission only for those frequencies above the plasma frequency for which the wave number is real. For this geometry of rods we have calculated the plasma

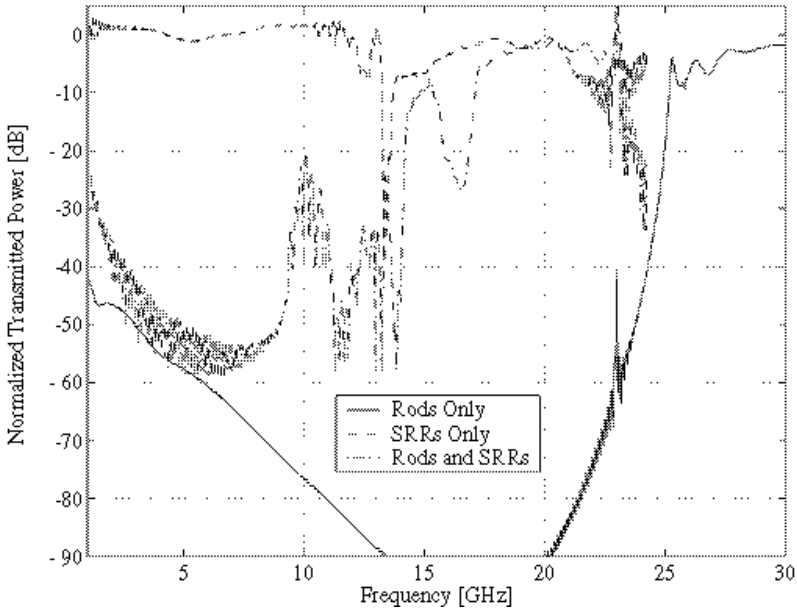

Figure 4. Normalized transmitted power through a metamaterial slab without dielectric (Type 1).

frequency to be 26 GHz, which matches well with the experiment. The structure with the rings alone has a significant effect on the propagating waves around resonance. According to [6], there are regions of positive and negative permeability on either side of the resonance. In the area of negative permeability, we expect that the fields within the SRRs are strong and in the same direction as the propagating field. The field outside the rings (i.e. the return field) is in the opposite direction and opposes the propagating field. At resonance, there is a narrow stop band, 30 dB down at approximately 13 GHz. Outside of resonance, the SRRs have little effect on the propagating field, their size being much less than one wavelength. Finally, for both rods and SRRs together, it is found that a small passband exists between 14 and 16 GHz, near the resonance of the rings. We note that there are other frequency ranges that are pass bands, but these are not near the resonance of the rings, so they are identified as other band gap phenomena of the metamaterial structure. There is also noise in the data due to the finite time of the FDTD simulation, since the structure is still 'ringing' slightly when the simulation is terminated at 16384 time steps. Longer simulations have been investigated, and we have determined that this truncation error does not affect the general characteristics of the data.

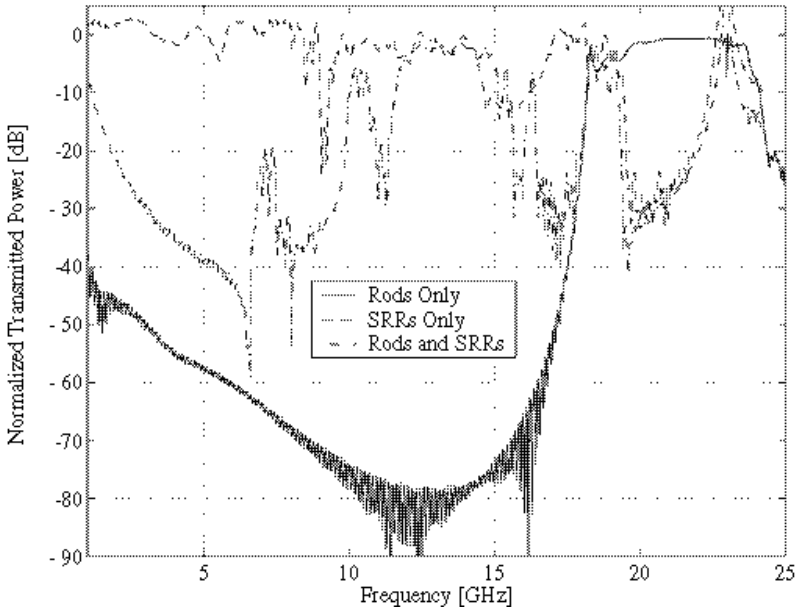

Figure 5. Normalized transmitted power through a metamaterial slab with dielectric (Type 2).

In addition, the higher frequency portions of the transmitted fields have noise due to both the truncated data and also the beginning of numerical dispersion. For these reasons, the high frequency portions of the transmission data for the SRRs and the complete structure have been truncated at 24 GHz.

Figure 5 shows the transmitted power for the Type 2 structure. The presence of the dielectric shifts the resonant frequencies down, as is expected from simple physical arguments. The stop band due to the SRR resonance occurs at 9 GHz and the transmitted signal is attenuated by 20 dB. A passband for the metamaterial structure is between 10 and 11 GHz, and is 7 dB down.

Figure 6 shows the transmitted power for the Type 3 structure. The resonance of the SRRs is still at 9 GHz, resulting in a 20 dB stop band. The passband is between 9 and 10 GHz, and is approximately 3 dB down from full transmission. From these results, it appears that the SRRs and rods in the $(\hat{y}, \hat{z})$ plane are not strictly required, which is expected given that incident field has a much stronger H_y field than an H_x field.

Finally, in Figure 7, the transmission data for the Type 4 structure are shown. The Type 4 structure has very similar transmission

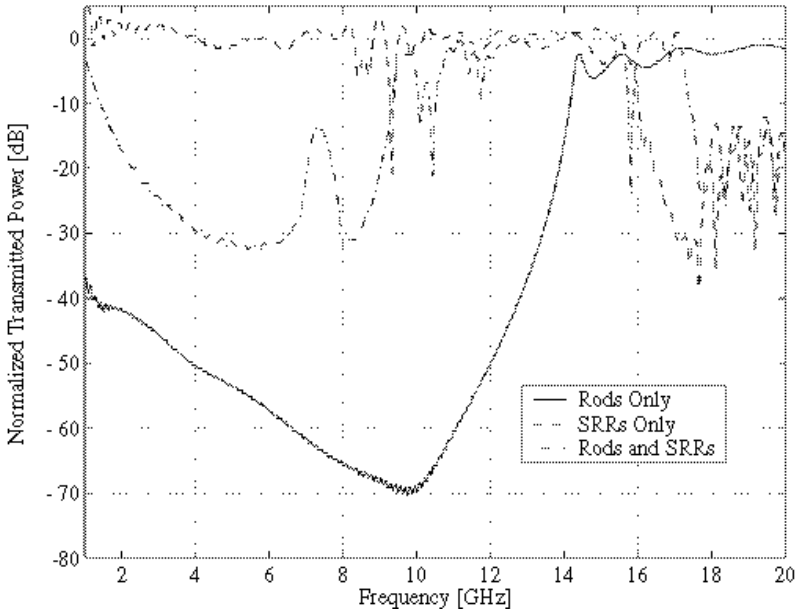

Figure 6. Normalized transmitted power through a metamaterial slab containing only SRRs in the $(\hat{z},\hat{y})$ plane with dielectric (Type 3).

characteristics to the previous three types of structures, indicating that the SRR model of Figure 2(b) is valid. For that case, the resonance of the SRRs is located around 16 GHz, attenuating the transmitted field by 30 dB. The passband occurs between 17 and 18 GHz, and is 10 dB down.

These results demonstrate that wideband examination of the metamaterial's transmission coefficients reveals separate characteristics of negative permittivity and permeability predicted by theoretical models and previous experimental studies. Given that the SRRs create an effective negative permeability near resonance, we focus on the nearby passbands in the combined SRR and rod structure to determine if left-handed properties exist.

3.2. Phase Data in an LH Metamaterial Slab

Another method of determining the LH property of a metamaterial is to measure the phase of a propagating wave inside the structure and look for the predicted backward phase velocity. Although such a phase measurement is difficult to perform in experimental settings (as the probe could couple with the structure), it is simple to do in numerical

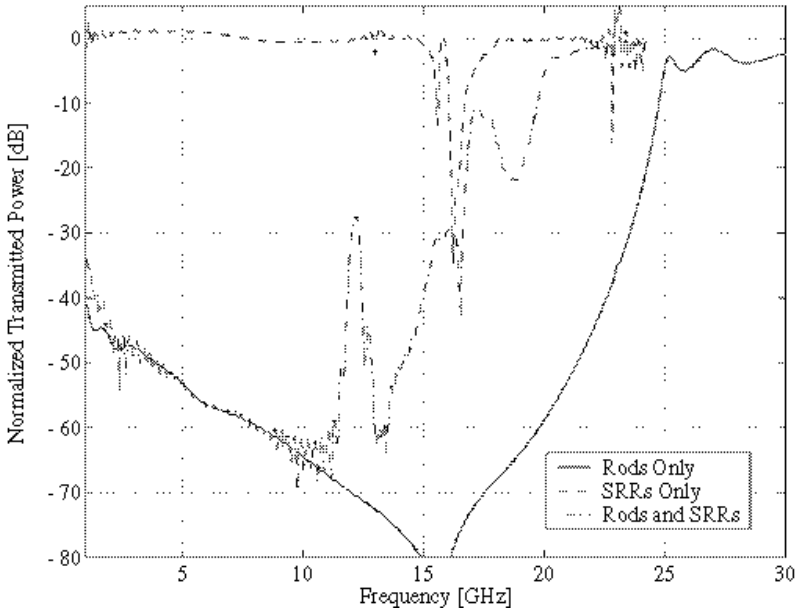

Figure 7. Normalized transmitted power through a metamaterial slab without dielectric (Type 4).

simulations.

In the frequency regime of negative permeability, an SRR produces a strong internal magnetic field that is in the same direction as the incident field. It is the external, or return field, that opposes the incident magnetic field and thus produces an effective negative permeability. The SRRs are in an array so that they approximate the effect of longer, continuous structures like cylinders (to produce a solenoid magnetic field) [6]. Hence we expect that the structure exhibits negative permeability external to the SRR rows, where the following phase data is obtained.

Figure 8 shows the absolute value of the electric field plotted along the center of the Type 1 structure. Although not included here due to space limitations, the magnetic field behaves similarly (between the rings). The vertical axis of the plot corresponds to the distance through the structure, which begins at $x = 6.75\,\text{mm}$ and ends at $x = 42\,\text{mm}$, and the horizontal axis of the plot is time, in nanoseconds. The field is a continuous waves (CW), ramped up with a Gaussian modulation and shown here in late time where the structure has reached steady state. We assume that the electric field can then be expressed as

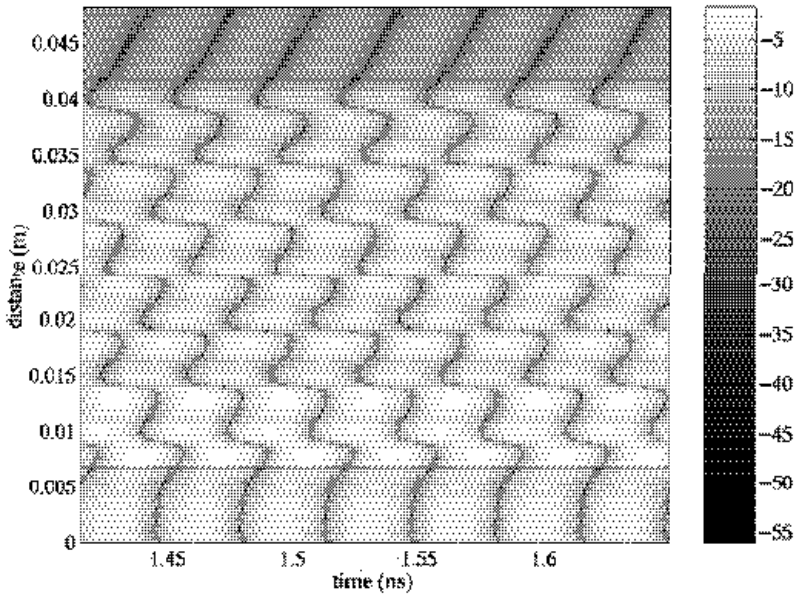

Figure 8. Absolute value of the electric field through the center of the Type 1 metamaterial, at 14.75 GHz (dB scale).

$E_z = \cos(kx - \omega t)$ for which a point of constant phase C results in $x = \frac{\omega}{k}t + \frac{C}{k}$.

The visually identifiable constant phase in Figure 8 is the null, which can be tracked through the structure. The slope of this phase is the phase velocity, $v_p = \omega/k$. The results shows that v_p is generally negative within the structure, but with positive slopes in regions close to the SRRs. As the wave exits the structure and enters free space, the phase velocity becomes positive. The field in the region of $x < .00675$ m contains both the incident field and the field reflected from the metamaterial structure, which explains the weaker positive slope of v_p than that of $x > 0.042$ m.

The actual phase velocity of the propagating field can be determined simply by extracting the slope of constant phase on any space-time plot similar to Figure 8. Although the null is visually obvious, it is numerically easier to calculate the slope from a maximum or minimum. Once the slope is found, we can determine a normalized v_p of the field and, given the assumption that the phase has the form $kx - \omega t$, also determine the index of refraction as $n = c/v_p$.

Figure 9 shows the calculated index of refraction, n_1, through the Type 1 structure for the electric field at 14.75 GHz. The phase

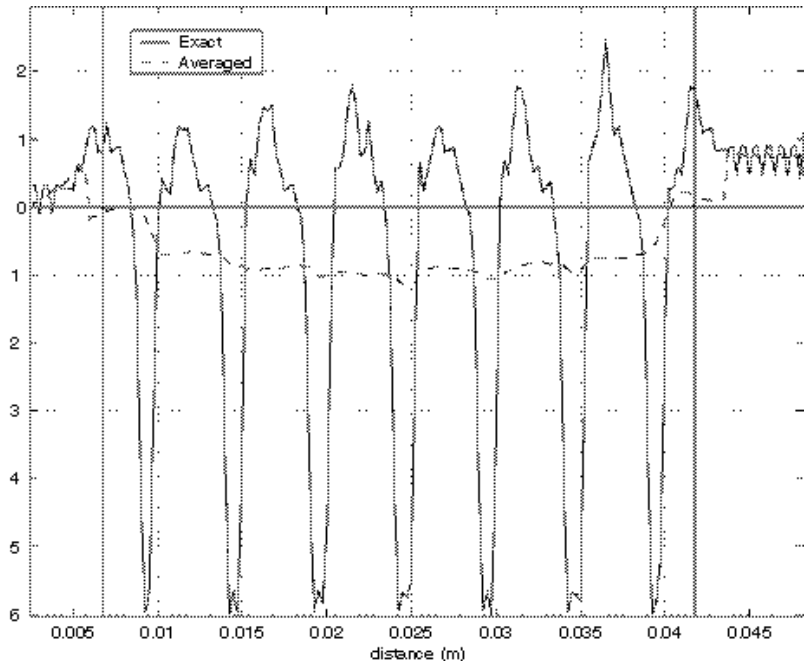

Figure 9. Exact and averaged (over 20 values) index of refraction through Type 1 metamaterial, at 14.75 GHz.

fluctuates as the field passes near an SRR, and n_1 briefly becomes positive. To achieve a better representation of the overall phase, an effective n_1 is calculated with an averaging window around each data point (in this case 20 values). The effective normalized n_1 in this structure is fairly constant, around $n_1 = -1$. Note however that there are edge effects at the beginning and the end of the metamaterial structure, where n_1 makes a transition from positive to negative ($x = 0.00675\,\mathrm{m}$) and back again ($x = 0.042\,\mathrm{m}$).

Figure 10 shows the averaged n_1 for different frequencies in the Type 1 structure. The metamaterial is very dispersive and inhomogeneous. In Figure 10, n_1 can be seen to become less negative as the frequency is increased from 14.5 GHz to 15 GHz, which is due to the narrow frequency band over which the material exhibits LH properties. Outside of that frequency band, n_1 becomes very irregular and eventually the structure no longer allows a propagating field (as the permeability becomes positive).

The averaged data of n_1 is dependent on the averaging window, and assumes the form of $kx - \omega t$ for the phase. To obtain another

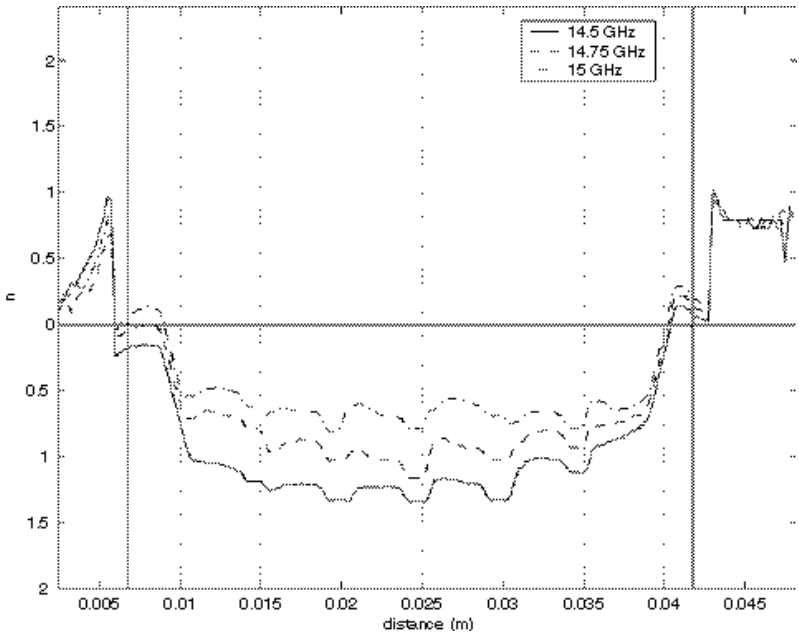

Figure 10. Index of refraction through Type 1 metamaterial for different frequencies.

measure of the phase behavior, the cumulative phase shift, $\Delta\psi$, for a continuous wave propagating through the structure can also be calculated. Table 1 shows the cumulative phase shift for various frequencies in the three types of metamaterial. The phase shift is calculated for 14.5 GHz to 15.5 GHz in the Type 1 structure, with a maximum shift of -3.7π at 14.5 GHz. At smaller frequencies, the phase could not me determined as the transmission through the structure became irregular. At 15 GHz, the phase shift through the Type 1 structure is approaching zero, and the transmitted power is decreasing as we approach the upper limit of the LH pass-band behavior. In the absence of the metamaterial, the free space phase shift (kd) would be 3.5π for 15 GHz. The same behavior can be seen in $\Delta\psi$ for the Type 2 structure, for frequencies from 10 GHz to 11 GHz, and for the Type 3 structure, for frequencies from 9.25 GHz to 10.25 GHz.

Figure 11 shows the power through the Type 1 structure at 14.75 GHz (above the middle SRR). The small regions of backward power are blacked out, and the system has a forward time average power propagation.

The results in this section were taken through the center of

Table 1. Total phase shift $\Delta\psi$ through the three types of LH metamaterials.

Type 1		Type 2		Type 3	
Freq. [GHz]	$\Delta\psi$	Freq. [GHz]	$\Delta\psi$	Freq. [GHz]	$\Delta\psi$
14.5	-3.7π	10	-3.3π	9.5	-4.0π
14.75	-2.9π	10.25	-3.5π	9.75	-2.8π
15	-2.2π	10.5	-2.0π	10	-2.2π
15.25	-1.5π	10.75	-1.4π	10.25	-1.5π
15.5	-0.9π	11	-0.5π	10.5	-0.3π

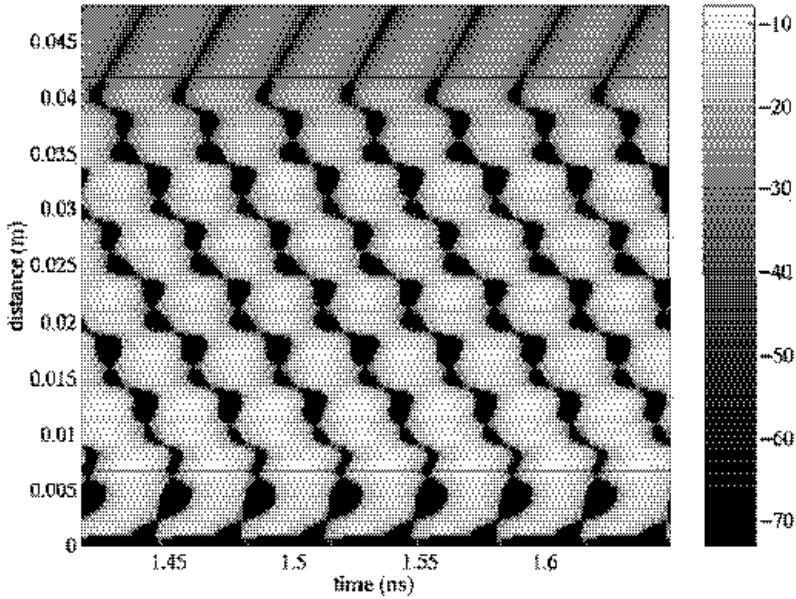

Figure 11. Power through the center of the Type 1 metamaterial, at 14.75 GHz (dB scale). Regions of backward (negative) power are blacked out.

the structure, and show an inhomogeneous behavior in the direction of propagation. In fact, the metamaterials are also spatially inhomogeneous in the plane transverse to the direction of propagation, and data shown here are only representative of the fields in the center of the structure. Edge effects are apparent near the microwave absorber and particularly strong near the waveguide plates. The field inhomogeneities near the waveguide plate are due the the asymmetry of the structure's image (when image theory is applied to account for effects of the waveguide).

3.3. Index of Refraction Calculated with an LH Metamaterial Prism

Another method of demonstrating LH behavior of a material is to construct a prism and calculate the direction of power leaving the structure. This has been carried out experimentally [8], and, to our knowledge, it is here for the first time rigorously verified with a numerical approach. Figure 12 shows the possibilities of Poynting vectors for power leaving a prism of various values of n_1. Upon measuring the direction of the power ($\overline{S}$) leaving the prism, it is possible to calculate the index of refraction using Snell's law.

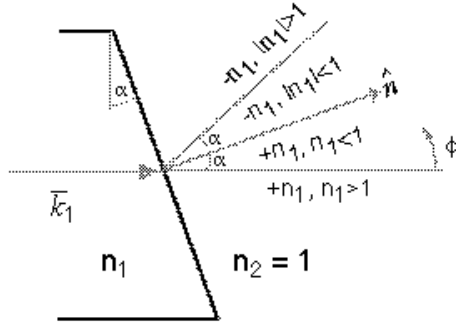

Figure 12. Possible directions of propagation for waves leaving a prism of material ϵ_1 into free space.

First we examine the direction of $\bar{S}$ leaving a prism of homogeneous dielectric ($\epsilon_r = 3.4$). A staircased approximation of $\alpha = 18.4°$ interface is used to model the prism. To determine the direction of the fields leaving the prism, we integrate the electric and magnetic fields over the aperture of the waveguide and calculate the far fields using Huygens' principle [15]. In this case $\overline{S} = \overline{E} \times \overline{H} = E_\theta \hat{\theta} \times H_\phi \hat{\phi} = S_r \hat{r}$. A pulse is used as the excitation, and the far fields

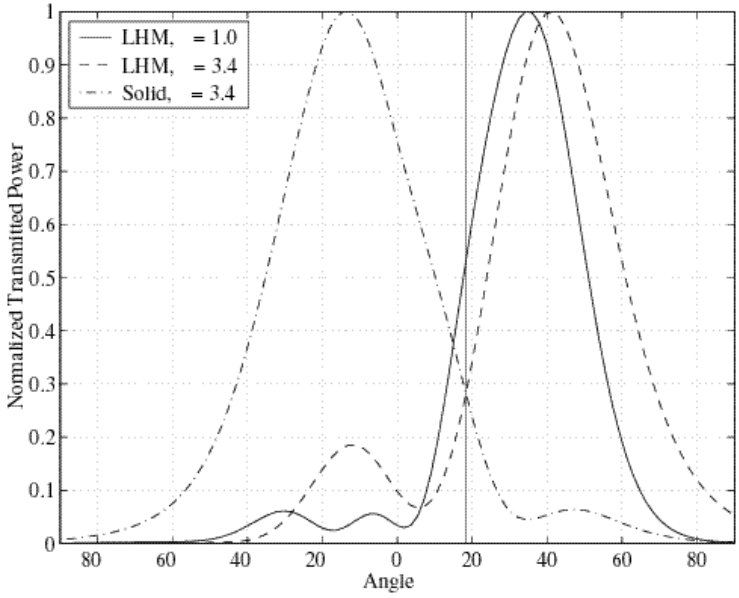

Figure 13. Far field power from prism (of various materials) vs azimuthal angle, $\alpha = 18.4^o$.

are calculated at the frequencies determined in the previous section. The quantity $S_r\hat{r}$ models the measurements that would be taken with a horn antenna moved along a radial axis, varying ϕ and keeping $\theta = \pi/2$. The results for $S\hat{r}$ in Figure 13 show the fields propagating in the $\phi = -14.5^\circ$ direction, which corresponds to a $\epsilon_r = 2.96$, or $n_1 = 1.72$ in the prism. The reason for this inaccuracy is the slightly non uniform (curved) phase front of the propagating field. Hence, this technique does not provide an exact way to determine n_1 of the prism, but is instead an approximation. The result can be an under-prediction of n_1, as one side of the curved phase front is almost parallel to the prism interface, whereas the other side may reach cut-off. Larger arrays of unit cells would alleviate this problem.

In order to build a metamaterial prism, we again use a coarse staircasing approximation, now with the metamaterial unit cells (Figure 3). To build the $\alpha = 18.4^\circ$ interface, we use three SRRs in $\hat{y}$ for every single SRR in $\hat{x}$. The far field plots are also shown in Figure 13 for the Type 1 and Type 2 metamaterials. The Type 1 metamaterial refracts the 14.75 GHz component of the pulse at an angle of $\phi = 35^\circ$, which corresponds to $n_1 = -0.91$. The Type 2 metamaterial refracts the 10.25 GHz component of the pulse at $\phi = 41^\circ$, which corresponds

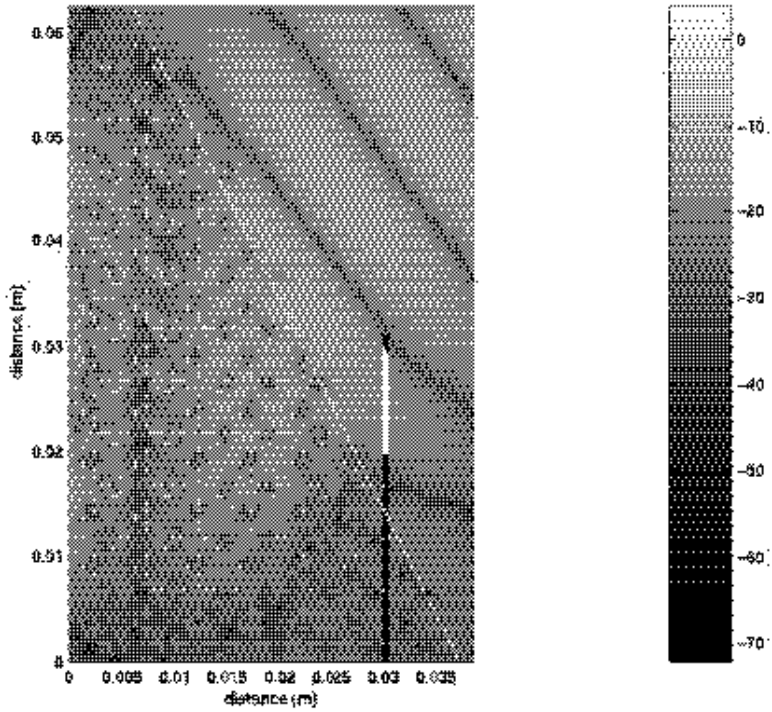

Figure 14. Absolute value of the electric field inside a metamaterial prism structure (dB scale), $\alpha = 26.6^o$.

to $n_1 = -1.2$. The metamaterials refract smaller amounts of power around 0°, which is likely due to non-uniform phase front of the incident wave as well as edge effects (apparent in Figure 14). The results in this section are consistent with the results in the previous section, where the index of refraction was calculated directly from the phase velocity within a metamaterial slab. In both sections, the Type 1 metamaterial index of refraction is approximately −1, and the Type 2 metamaterial's index of refraction is approximately −1 to −1.5.

For visualization purposes, Figure 14 shows the electric field of a continuous wave leaving a prism of larger angle ($\alpha = 26.6°$), and one can see the phase fronts indicative of a field refracted from a negative medium into a positive one (free space in this case). The metallization of the metamaterial is indicated in white on the plot, as is the approximate prism boundary (for illustration).

4. CONCLUSION

This work examined three techniques to localize and demonstrate the LH behavior of a metamaterial. First, the possible frequency band of LH behavior was determined by calculating the transmitted power of a wideband pulse through the metamaterial. In that frequency band, the backward phase velocity in a slab of metamaterial was then verified, and the index of refraction was calculated. At the same frequencies, a negative index of refraction was demonstrated by calculating the direction of power leaving a metamaterial prism. The two methods of calculating the index of refraction of the metamaterials gave consistent results. The FDTD model in this work uses two different SRR geometries, one that is optimal for the uniform Cartesian grid, and the other that is a model of geometries used in previous experiments [8]. The numerical study enables a greater understanding of the phenomena that leads to LH behavior in metamaterials, and can be easily changed to examine new metamaterial geometries in the future. To our knowledge, this is the first time that the LH properties of metamaterials have been verified and studied using a full wave numerical model of an entire experimental geometry.

ACKNOWLEDGMENT

This work was supported by MIT Lincoln Laboratory contract BX-8133 and also by the Office of Naval Research under contracts N00014-10-1-0713 and N00014-99-1-0175.

REFERENCES

1. Smith, D. R., W. J. Padilla, D. C. Vier, D. C. Nemal-Nasser, and S. Schultz, "Composite medium with simultaneously negative permeability and permittivity," *Phys. Rev. Lett.,* Vol. 84, No. 18, May 2000.
2. Kong, J. A., "Electromagnetic wave interaction with stratified negative isotropic media," *J. Electromagnetic Waves and Applications,* Vol. 15, No. 10, 2001.
3. Veselago, V. G., "The electrodynamics of substances with simultaneously negative values of ϵ and μ," *Soviet Physics,* Vol. 10, No. 4, January 1968.
4. Pendry, J. B., "Negative refraction makes a perfect lens," *Phys. Rev. Lett.,* Vol. 85, No. 18, October 2000.
5. Rotman, W., "Plasma simulation by artificial dielectrics and

parallel-plate media," *IRE Trans. Antennas and Propagation,* Vol. AP-10, 82–95, January 1962.

6. Pendry, J. B., A. J. Holden, D. J. Robbins, and W. J. Stewart, "Low frequency plasmons in thin wire structures," *J. Phys. Condens. Matter,* Vol. 10, No. 22, 4785–4809, June 1998.
7. Pendry, J. B., A. J. Holden, D. J. Robbins, and W. J. Stewart, "Magnetism from conductors and enhanced nonlinear phenomena," *IEEE Trans. Microwave Theory Tech.,* Vol. 47, No. 11, November 1999.
8. Shelby, R. A., D. R. Smith, and S. Schultz, "Experimental verification of a negative index of refraction," *Science,* Vol. 292, April 2001.
9. Kong, J. A., B.-I. Wu, and Y. Zhang, "Lateral displacement of a Gaussian beam reflected from a grounded slab with negative permittivity and permeability," *Appl. Phys. Lett.,* Vol. 80, No. 12, March 2001.
10. Caloz, C., C.-C. Chang, and T. Itoh, "Full-wave verification of the fundamental properties of left-handed materials in waveguide configurations," *Journal of Applied Physics,* Vol. 90, No. 11, 5483–5486, December 2001.
11. Markos, P., and C. M. Soukoulis, "Transmission studies of left-handed materials," *Physical Review B,* Vol. 65, December 2001.
12. Weiland, T., R. Schuhmann, R. B. Greegor, C. G. Parazzoli, A. M. Vetter, D. R. Smith, D. C. Vier, and S. Schultz, "*Ab initio* numerical simulation of left-handed metamaterials: Comparison of calculations and experiments," *Journal of Applied Physics,* Vol. 90, No. 10, 5419–5424, November 2001.
13. Berenger, J. P., "A perfectly matched layer for the absorption of electromagnetic waves," *J. Comp. Phys.,* Vol. 114, 185–200, 1994.
14. Harris, F. J., "On the use of windows for harmonic analysis with discrete Fourier Transform," *Proc. IEEE,* Vol. 66, 51–83, 1978.
15. Kong, J. A., *Electromagnetic Wave Theory,* Second edition, John Wiley & Sons, Inc., New York, 1990.